Applied Physics Letters

Tuning the electronic properties of epitaxial strained $CaFeO_{3-\delta}$ thin films

Cite as: Appl. Phys. Lett. **114**, 221907 (2019); https://doi.org/10.1063/1.5098025
Submitted: 30 March 2019 . Accepted: 15 May 2019 . Published Online: 07 June 2019

Tongtong Huang, Yujia Wang, Haobo Li, Meng Wang, Yingjie Lyu, Shengchun Shen, Nianpeng Lu, Qing He, and Pu Yu

Applied Physics Letters ARTICLE scitation.org/journal/apl

Tuning the electronic properties of epitaxial strained $CaFeO_{3-\delta}$ thin films

Cite as: Appl. Phys. Lett. **114**, 221907 (2019); doi: 10.1063/1.5098025
Submitted: 30 March 2019 · Accepted: 15 May 2019 ·
Published Online: 7 June 2019

Tongtong Huang,[1] Yujia Wang,[1] Haobo Li,[1] Meng Wang,[1] Yingjie Lyu,[1] Shengchun Shen,[1] Nianpeng Lu,[1] Qing He,[2] and Pu Yu[1,3,a)]

AFFILIATIONS

[1]State Key Laboratory of Low Dimensional Quantum Physics and Department of Physics, Tsinghua University, Beijing 100084, China
[2]Department of Physics, Durham University, Durham DH13LE, United Kingdom
[3]RIKEN Center for Emergent Matter Science (CEMS), Saitama 351-0198, Japan

[a)]Email: yupu@tsinghua.edu.cn

ABSTRACT

Strain engineering of transition metal oxides due to their desirable properties has long been a focal point in both physics and material sciences. Here, we investigate the strain dependence of electronic and optical properties of the high valence iron-based perovskite $CaFeO_{3-\delta}$. Using substrates with various lattice constants, we achieve a wide range of tunable epitaxial strain states in $CaFeO_{3-\delta}$ thin films ranging from compressive −0.37% to tensile 3.58%. Electrical transport and optical absorption measurements demonstrate a distinct strain-dependent behavior, in which larger tensile strain leads to higher electrical resistivity and a larger optical bandgap. We attribute these modulations to tensile strain suppressed *p-d* hybridization in $CaFeO_{3-\delta}$, as evidenced by soft X-ray absorption spectra measurements.

Complex transition metal oxides have attracted extensive scientific interest in the last few decades due to their fascinating electrical and magnetic properties as well as their significant potential for application in energy storage/conversion, memory, etc.[1,2] To manipulate the intrinsic properties of complex oxides, many approaches have been proposed and investigated. One classical and effective way to control the crystalline structure is through the epitaxial strain in the thin film form, which can greatly modulate the distortion of the metal-oxide ligand to influence the corresponding material functionalities, such as electronic band structure, ferromagnetism, superconductivity, ferroelectricity, etc.[3–6]

As one prototypical iron-based perovskite, $CaFeO_3$ (P-CFO) exhibits several unique physical behaviors, including charge disproportionation with a metal-insulator transition, complex screw spin configuration, etc.[7–10] In addition, due to the existence of a high valence state in iron (Fe^{4+}), P-CFO is also a promising material candidate for catalytic[11] and battery applications,[12] where the electronic band structure plays an essential role in determining the corresponding properties. Due to the strong correlation between the exotic metal-insulator transition of P-CFO and its crystal structure, recently, strain engineering of oxygen stoichiometric P-CFO has attracted extensive research interests.[13] However, the understanding of the strain effect on its electronic band structure is still missing, especially for the slightly oxygen deficient P-CFO phase, which is essential for real applications.

In this work, we fabricate P-CFO epitaxial thin films with strain states ranging from −0.37% to 3.58% by using substrates with different lattice constants. In various strain states, all P-CFO thin films possess the same Fe valence state, while their physical properties are remarkably different. As the tensile strain increases, the resistivity of P-CFO is enhanced by up to 6 orders of magnitude at room temperature, and the corresponding optical bandgap demonstrates a blue shift of ∼0.6 eV. Soft X-ray absorption spectra of Fe *L*-edge and O *K*-edge indicate that these interesting phenomena can be attributed to the suppressed Fe 3*d* and O 2*p* hybridization along with increasing tensile strain. These results not only shed light on the exotic physical features of the P-CFO system, but also provide an effective pathway to engineer the material functionalities of complex oxides.

Conventionally, to obtain P-CFO, the thin film is usually grown in highly oxidizing environments with oxygen plasma or ozone.[13,14] In this work, we developed a two-step method instead to achieve P-CFO from the oxygen deficient brownmillerite $CaFeO_{2.5}$ (BM-CFO). Firstly, BM-CFO thin films were fabricated on various (001) oriented substrates including $SrTiO_3$ (STO, $a = 3.905$ Å), $(LaAlO_3)_{0.3}$-$(SrAl_{0.5}Ta_{0.5}O_3)_{0.7}$ (LSAT, $a = 3.868$ Å), $LaAlO_3$ (LAO, $a = 3.790$ Å), and $LaSrAlO_4$ (LSAO, $a = 3.756$ Å)

(see the supplementary material for details). As shown in Fig. 1(a), the initial growth orientations of epitaxial BM-CFO thin films depend on the selection of substrates, in which the ordered oxygen deficient channels are formed along the in-plane and out-of-plane directions under tensile and compressive strain, respectively.[15–17] These crystal orientations were verified by the presence of superlattice peaks only in the tensile strained samples as shown in Fig. S1, which is due to the alternative stacking of the oxygen octahedra and tetrahedra along the out-of-plane direction. With these high-quality BM-CFO thin films, a postozone annealing process was carried out to trigger the phase transformation from brownmillerite to the perovskitelike phase P-CFO (see the supplementary material for details). Despite the different oxygen vacancy orientations in pristine BM-CFO under different strain states, all of them can be completely transformed into a perovskite structure after annealing, with tetrahedral FeO_4 oxidized to octahedral FeO_6. As shown in Fig. 1(b), the films on different substrates exhibit only (001) and (002) diffraction peaks of the pseudocubic lattice, indicating the formation of P-CFO phases. The reciprocal space maps (RSM) shown in Fig. 1(c) demonstrate that all films are coherently strained with their substrates. Figure 1(d) summarizes the tetragonality ratio c/a and unit cell volumes versus nominal in-plane lattice mismatch $\varepsilon = (a_s - a_f)/a_f$, where a_s and a_f are the in-plane lattice constants of the pseudocubic substrates and bulk P-CFO [$a = 5.326$, $b = 5.353$, $c = 7.540$, $a_f = 3.770$ Å (Ref. 7)], respectively. This plot clearly reveals that the tetragonality of P-CFO films decreases systematically with increasing tensile strain, while the lattice volumes increase from 53.47 (P-CFO/LSAO) to 56.51 (P-CFO/STO) Å (Ref. 3). It is important to note

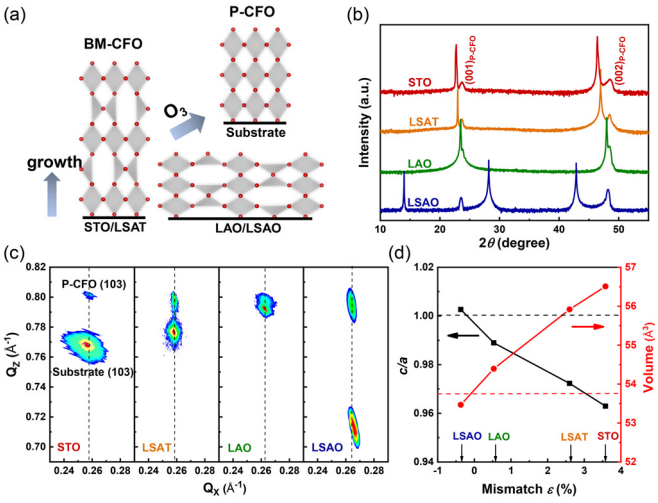

FIG. 1. (a) Schematic illustration of the strategy to obtain perovskite $CaFeO_{3-\delta}$ (P-CFO) from brownmillerite $CaFeO_{2.5}$ (BM-CFO) through postozone annealing. The BM-CFO thin films show different crystalline orientations depending on the epitaxial strain state. (b) X-ray 2θ-ω scans for P-CFO thin films grown on STO (001), LSAT (001), LAO (001), and LSAO (001) substrates. (c) Reciprocal space maps for P-CFO thin films grown on STO, LSAT, LAO, and LSAO around their pseudocubic (103) Bragg reflection. (d) Evolution of the tetragonality (c/a) and the pseudocubic unit cell volume for different P-CFO thin films along with the in-plane lattice mismatch on different substrates.

that the bulk unit cell volume of 53.74 Å (Ref. 3) (guided with the red dashed line) agrees nicely with the experimental trend, suggesting good stoichiometry of P-CFO samples. The expanded volume for tensile samples should be attributed to a nonelastic lattice distortion with the Poisson ratio of ∼0.15, which has been observed in similar complex oxide systems.[18,19]

In order to investigate the strain effect on the electrical properties of the P-CFO system, electrical transport measurements were carried out. Unfortunately, metal-insulator transition was not observed in our samples, which may be due to the small amount of oxygen vacancies formed in our $CaFeO_{3-\delta}$ samples. While the temperature (T) dependent resistivity (ρ) as presented in Fig. 2(a) reveals a clear exponential increase with decreasing temperature for all strained thin films, which can be recognized as a typical characteristic behavior for semiconductors.[20] Furthermore, the epitaxial strain exhibits a remarkable influence on the electronic transport properties, where the resistivity of P-CFO/STO and P-CFO/LAST under large tensile strain is about 4–6 orders of magnitude higher than that on LAO and LSAO [inset of Fig. 2(a)]. The ρ-T behavior above 200 K follows the thermally activated small polaron hopping (SPH) model,[21–24] described by[25]

$$\rho/T = \rho_\alpha \exp(E_p/k_B T), \tag{1}$$

where k_B and T are the Boltzmann constant and the absolute temperature, respectively. And,

$$\rho_\alpha = [k_B/\nu_{\mathrm{ph}} N e^2 R^2 C(1-C)] \exp(2\alpha R), \tag{2}$$

where N, $R \sim (1/N)^{1/3}$, C, α, and ν_{ph} denote the number of ion sites per unit volume, the average intersite spacing, the fraction of sites occupied by a polaron, the electron wave function decay constant, and the optical phonon frequency, respectively. Thus, the small polaron activation energy (E_p) was determined from the slope of the $\ln(\rho/T)$ vs $1/T$ curve [Fig. 2(b)], which is 60.4, 77.8, 223.1, and 228.8 meV for LSAO, LAO, LSAT, and STO, respectively, showing a systematic enhancement along with the increase in tensile strain.

To further study the electronic structure of the P-CFO thin films, optical transmittance measurements were performed at room temperature. The spectra [Fig. 3(a)] reveal two distinct transmittance valleys at ∼500 and ∼1400 nm, corresponding to two absorption peaks at ∼2.5 and ∼0.75 eV marked by the triangle and the star in the inset,

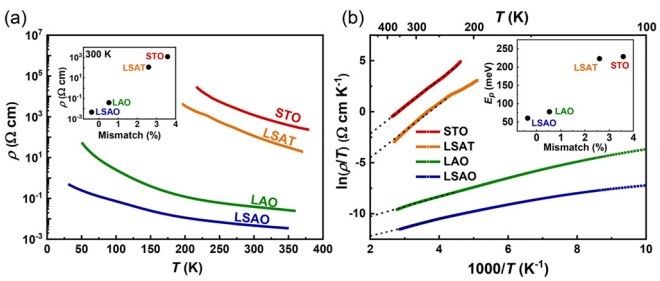

FIG. 2. (a) Temperature dependent electrical resistivity measurements of P-CFO thin films grown on different substrates. The inset shows a direct comparison of room temperature resistivities among all four samples. (b) $\ln(\rho/T)$ vs $1/T$ plots of P-CFO thin films grown on different substrates. Dark dashed lines are fittings of experimental data with the small polaron hopping model. The inset shows strain dependent E_p obtained from the fitting.

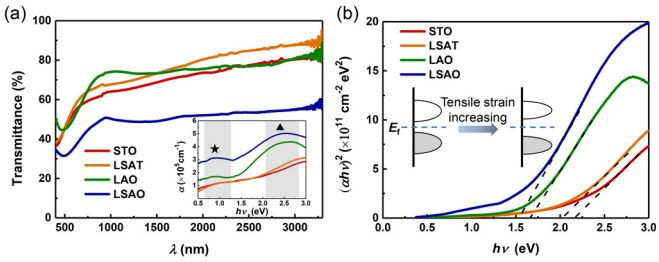

FIG. 3. (a) Optical transmittance spectra in the visible and near-infrared regions of P-CFO thin films grown on different substrates. The inset shows the corresponding absorption spectrum $\alpha(h\nu)$, where the gray shaded areas indicate the absorption peaks around 0.75 eV and 2.5 eV, labeled as the star and the triangle, respectively. (b) $(\alpha h\nu)^2$ vs $h\nu$ plots of the absorption spectra. We obtained the optical (direct) bandgap from the intercepts of these fitting dashed lines on the energy axis, which are 1.53, 1.64, 2.03, and 2.14 eV for the P-CFO film on LSAO, LAO, LSAT, and STO, respectively. The inset shows a schematic illustration of the evolution of bandgap with the increase of tensile strain.

which can be attributed to the charge transfer transition from the O 2*p* orbitals to the Fe 3*d* orbitals, and the intraband transition between the Fe 3*d* orbitals, respectively.[9] In order to estimate the electronic direct (optical) bandgap, we replot the data into Tauc plots as shown in Fig. 3(b), in which the absorption edge follows the equation[26]

$$(\alpha h\nu)^2 = A(h\nu - E_g), \tag{3}$$

where A, α, h, ν, and E_g are the prefactor, optical absorption coefficient, Planck constant, photon frequency, and the direct bandgap, respectively. From this fitting, the direct bandgaps for all four strained P-CFO thin films are estimated as 1.53, 1.64, 2.03, and 2.14 eV, respectively, with the higher strain corresponding to a larger bandgap.

To shed light on the electronic structure evolution with epitaxial strain, we further investigated the valence state of the Fe ion in different strained P-CFO thin films by soft X-ray absorption spectroscopy (sXAS) at the Fe *L*-edge. Figure 4(a) displays the spectra of all P-CFO thin films (solid lines) along with two reference spectra (dotted lines) of $LaFeO_3$ and $SrFeO_3$ (SFO).[27] The P-CFO samples show almost identical absorption features with the L_3 peak located around 709.7 eV, which ascertains close oxygen stoichiometry among all these P-CFO films. As a comparison, the sXAS spectrum of BM-CFO shows a distinct line-shape with a characteristic pre-edge peak at ~708.2 eV and a shift of the L_3 peak to ~709.4 eV (see Fig. S3). The stark different spectra between these two cases again confirm a valence change from Fe^{3+} to Fe^{4+} during the ozone postannealing. However, we also observe a small pre-edge peak from the sXAS spectra of P-CFO samples as compared with that of SFO, which could be attributed to the slight oxygen nonstoichiometry in P-CFO. To directly probe the O 2*p*-Fe 3*d* orbital hybridization, we measured subsequently the O *K*-edge absorption spectra, as shown in Fig. 4(b), in which we could identify a series of distinct features (labeled as A, B, and C) in the pre-edge region. The inset in Fig. 4(b) shows a schematic diagram of the O pre-edge spectrum for the Fe $3d^4$ band hybridized with O 2*p* orbitals. Feature A (~527.9 eV) corresponds to the hybridization with the unoccupied spin-up e_g band in the nominal Fe^{4+} (t_{2g}^3 e_g^1) and the splitting of features B and C can be interpreted as the energy difference between the spin-down t_{2g} and spin-down e_g bands due to the crystal field.[28–30]

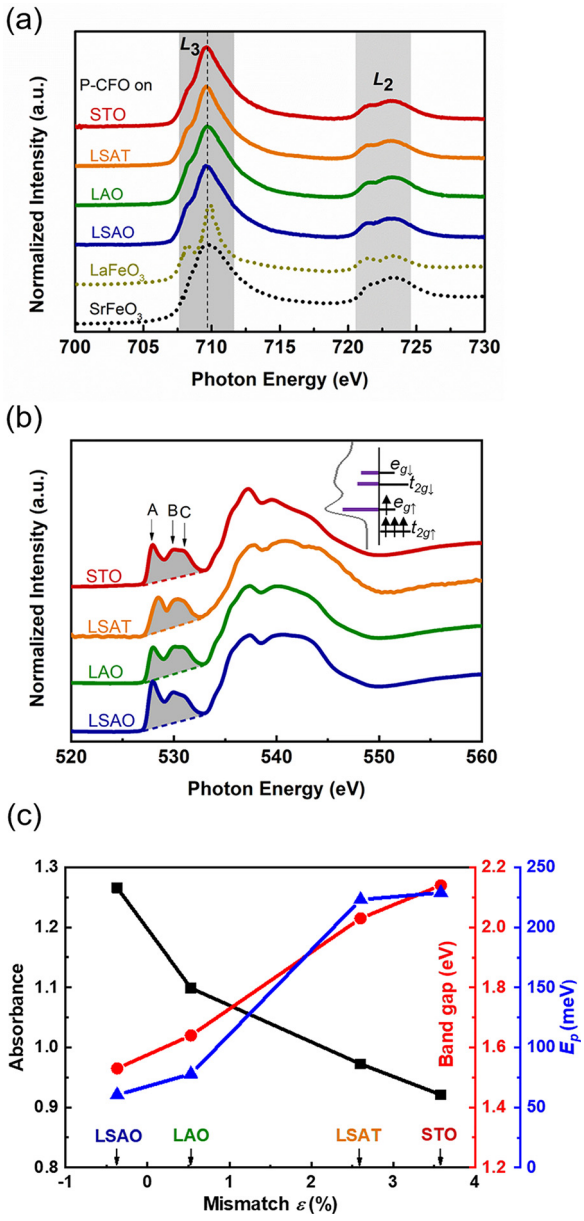

FIG. 4. (a) Fe *L*-edge (300 K, TEY mode) and (b) O *K*-edge soft X-ray absorption spectra (20 K, TEY mode) of the P-CFO thin films grown on different substrates. (c) Integration of the shaded area (absorbance, back dots) in the pre-edge of O *K*-edge absorption spectra. The optical bandgap (red dots) and the activation energy E_p (blue dots) are also summarized for comparison.

Therefore, the strength of *p*-*d* hybridization (β^2) can be estimated as the intensity of the pre-edge (i.e., ligand-hole) spectra, normalized by the density of O 2*p*-Fe 3*d* unoccupied states, and is quantified as:[31]

$$|\beta|^2 \propto \text{Absorbance}/(\text{hole}_{eg} + {}^1\!/_4\,\text{hole}_{t2g}), \tag{4}$$

where the absorbance can be estimated by the integration of pre-edge spectra (shaded area) after background linear subtraction shown in Fig. 4(b) and the holes for e_g and t_{2g} are defined by the nominal

unoccupied density of states for the e_g and t_{2g} orbitals, respectively. The prefactor 1/4 for the t_{2g} hole accounts for the transfer integral difference between t_{2g} and e_g. With these, we obtained the *p-d* hybridization strengths for the P-CFO thin films on different substrates as summarized in Fig. 4(c), which indicate that the increasing tensile strain leads to weaker *p-d* hybridization. To further understand the evolution of *p-d* hybridization, we expect the lattice distortion of FeO_6 octahedra in P-CFO to play an important role in determining the strength of hybridization. In iron-based perovskite oxides, such as SFO and P-CFO, the orbital hybridization between O:2*p* σ and Fe:3*d* e_g leads to the formation of the σ^* band, in which the bandwidth (W_{σ^*}) is directly influenced by the geometry of FeO_6 octahedra.[7,32] For SFO with no distortion, corresponding to a wider σ^* band and higher hybridization, it exhibits a metallic behavior.[32,33] While due to the smaller ionic radius of Ca^{2+}, which induces more intensive distortion of FeO_6 octahedra, P-CFO processes much higher resistivity with an exotic metal-insulator transition at a lower temperature.[34,35] The observations of weakened hybridization in highly tensile strained P-CFO are closely correlated to the intensively distorted Fe-O ligands, evidenced by the changes of tetragonality and lattice volume. With increasing tensile strain, the out-of-plane lattice constants are reduced systematically as well as stronger distortion of FeO_6 octahedra, which narrows the σ^* band for strained P-CFO as compared with the bulk. Finally, owing to the suppressed *p-d* hybridization, the charge carrier becomes more localized, thus a larger energy E_p would be required to obtain the conducting carrier in these semiconductor samples.

In summary, we developed an effective approach to synthesize high quality P-CFO thin films with a large range of tunable epitaxial strain states. Systematic measurements of their electronic and optical properties reveal that the tensile strain leads to remarkably enhanced electrical resistivity and direct bandgap in P-CFO. We attribute these modulation effects to strain-manipulated *p-d* orbital hybridization, in which the larger tensile strain weakens the hybridization strength and suppresses the bandwidth. This study opens a pathway to engineer the electronic states in P-CFO and other complex oxides through bandwidth control, which would be of great benefit to the applications that take advantage of their tunable electronic states.

See the supplementary material for additional details of sample preparation and measurement methods.

This study was financially supported by the Basic Science Center Project of NFSC under Grant No. 51788104; the National Basic Research Program of China (Grant Nos. 2015CB921700 and 2016YFA0301004); the Beijing Advanced Innovation Center for Future Chip (ICFC); and the Engineering and Physical Sciences Research Council (Grant No. EP/N016718/1). This work made use of the resources at the Advanced Light Source supported by the U.S. Department of Energy under Contract No. DE-AC02-05CH11231.

REFERENCES

[1]A. S. Arico, P. Bruce, B. Scrosati, J. M. Tarascon, and W. Van Schalkwijk, Nat. Mater. **4**(5), 366 (2005).
[2]A. Sawa, Mater. Today **11**(6), 28 (2008).
[3]J. Nichols, J. Terzic, E. G. Bittle, O. B. Korneta, L. E. De Long, J. W. Brill, G. Cao, and S. S. A. Seo, Appl. Phys. Lett. **102**(14), 141908 (2013).
[4]Y. Takamura, R. V. Chopdekar, E. Arenholz, and Y. Suzuki, Appl. Phys. Lett. **92**(16), 162504 (2008).
[5]J. P. Locquet, J. Perret, J. Fompeyrine, E. Mächler, J. W. Seo, and G. Van Tendeloo, Nature **394**(6692), 453 (1998).
[6]J. W. Guo, P. S. Wang, Y. Yuan, Q. He, J. L. Lu, T. Z. Chen, S. Z. Yang, Y. J. Wang, R. Erni, M. D. Rossell, V. Gopalan, H. J. Xiang, Y. Tokura, and P. Yu, Phys. Rev. B **97**(23), 235135 (2018).
[7]P. M. Woodward, D. E. Cox, E. Moshopoulou, A. W. Sleight, and S. Morimoto, Phys. Rev. B **62**(2), 844 (2000).
[8]J. Matsuno, T. Mizokawa, A. Fujimori, Y. Takeda, S. Kawasaki, and M. Takano, Phys. Rev. B **66**(19), 193103 (2002).
[9]J. Fujioka, S. Ishiwata, Y. Kaneko, Y. Taguchi, and Y. Tokura, Phys. Rev. B **85**(15), 155141 (2012).
[10]C. X. Zhang, H. L. Xia, H. Liu, Y. M. Dai, B. Xu, R. Yang, Z. Y. Qiu, Q. T. Sui, Y. W. Long, S. Meng, and X. G. Qiu, Phys. Rev. B **95**(6), 064104 (2017).
[11]S. Yagi, I. Yamada, H. Tsukasaki, A. Seno, M. Murakami, H. Fujii, H. R. Chen, N. Umezawa, H. Abe, N. Nishiyama, and S. Mori, Nat. Commun. **6**, 8249 (2015).
[12]M. Hibino, R. Harimoto, Y. Ogasawara, R. Kido, A. Sugahara, T. Kudo, E. Tochigi, R. Shibata, Y. Ikuhara, and N. Mizuno, J. Am. Chem. Soc. **136**(1), 488 (2014).
[13]P. C. Rogge, R. U. Chandrasena, A. Cammarata, R. J. Green, P. Shafer, B. M. Lefler, A. Huon, A. Arab, E. Arenholz, H. N. Lee, T. L. Lee, S. Nemšák, J. M. Rondineli, A. X. Gray, and S. J. May, Phys. Rev. Mater. **2**(1), 015002 (2018).
[14]T. Akao, Y. Azuma, M. Usuda, Y. Nishihata, J. Mizuki, N. Hamada, N. Hayashi, T. Terashima, and M. Takano, Phys. Rev. Lett. **91**(15), 156405 (2003).
[15]M. D. Rossell, O. I. Lebedev, G. Van Tendeloo, N. Hayashi, T. Terashima, and M. Takano, J. Appl. Phys. **95**(9), 5145 (2004).
[16]S. Inoue, M. Kawai, N. Ichikawa, H. Kageyama, W. Paulus, and Y. Shimakawa, Nat. Chem. **2**(3), 213 (2010).
[17]J. Young and J. M. Rondinelli, Phys. Rev. B **92**(17), 174111 (2015).
[18]V. V. Mehta, N. Biskup, C. Jenkins, E. Arenholz, M. Varela, and Y. Suzuki, Phys. Rev. B **91**(14), 144418 (2015).
[19]I. C. Infante, F. Sánchez, J. Fontcuberta, M. Wojcik, E. Jedryka, S. Estradé, F. Peiró, J. Arbiol, V. Laukhin, and J. P. Espinós, Phys. Rev. B **76**(22), 224415 (2007).
[20]T. L. Phan, P. T. Tho, N. Tran, D. H. Kim, B. W. Lee, D. S. Yang, D. V. Thiet, and S. L. Cho, J. Electron. Mater. **47**(1), 188 (2018).
[21]A. Banerjee, S. Pal, and B. K. Chaudhuri, J. Chem. Phys. **115**(3), 1550 (2001).
[22]S. Mollah, H. L. Huang, H. D. Yang, S. Pal, S. Taran, and B. K. Chaudhuri, J. Magn. Magn. Mater. **284**, 383 (2004).
[23]D. Varshney and N. Dodiya, J. Theor. Appl. Phys. **9**(1), 45 (2015).
[24]J. Wang, F. X. Hu, Y. Y. Zhao, Y. Liu, R. R. Wu, J. R. Sun, and B. G. Shen, Appl. Phys. Lett. **106**(10), 102406 (2015).
[25]N. F. Mott and E. A. Davis, *Electronic Process in Non-Crystalline Materials* (Oxford University Press, 1971).
[26]J. I. Pankove, *Optical Processes in Semiconductors* (Courier Corporation, 1971).
[27]M. Abbate, F. M. F. De Groot, J. C. Fuggle, A. Fujimori, O. Strebel, F. Lopez, M. Domke, G. Kaindl, G. A. Sawatzky, M. Takano, Y. Takeda, H. Eisaki, and S. Uchida, Phys. Rev. B **46**(8), 4511 (1992).
[28]H. Wadati, A. Chikamatsu, R. Hashimoto, M. Takizawa, H. Kumigashira, A. Fujimori, M. Oshima, M. Lippmaa, M. Kawasaki, and H. Koinuma, J. Phys. Soc. Jpn. **75**(5), 054704 (2006).
[29]M. Abbate, G. Zampieri, J. Okamoto, A. Fujimori, S. Kawasaki, and M. Takano, Phys. Rev. B **65**(16), 165120 (2002).
[30]A. Braun, D. Bayraktar, S. Erat, A. S. Harvey, D. Beckel, J. A. Purton, P. Holtappels, L. J. Gauckler, and T. Graule, Appl. Phys. Lett. **94**(20), 202102 (2009).
[31]J. Suntivich, H. A. Gasteiger, N. Yabuuchi, H. Nakanishi, J. B. Goodenough, and Y. Shao-Horn, Nat. Chem. **3**(7), 546 (2011).
[32]J. B. Goodenough and J. S. Zhou, Chem. Mater. **10**(10), 2980 (1998).
[33]T. Takeda, R. Kanno, Y. Kawamoto, M. Takano, S. Kawasaki, T. Kamiyama, and F. Izumi, Solid State Sci. **2**(7), 673 (2000).
[34]M. Takano, N. Nakanishi, Y. Takeda, S. Naka, and T. Takada, Mater. Res. Bull. **12**(9), 923 (1977).
[35]S. Kawasaki, M. Takano, R. Kanno, T. Takeda, and A. Fujimori, J. Phys. Soc. Jpn. **67**(5), 1529 (1998).